Brodogradnja Volume 76 Number 1 (2025) 76106

journal homepage: www.brodogradnja.fsb.hr

Brodogradnja

An International Journal of Naval Architecture and Ocean Engineering for Research and Development

An adaptive NMPC for ROVs trajectory tracking with environmental disturbances and model uncertainties

Yi Zhang[1], *Jianing Zhang*[*1], *Zhiyang Guo*[1], *Lei Zhang*[1], *Yuchen Shang*[2]

[1] *School of Naval Architecture and Ocean Engineering, Dalian Maritime University, Dalian 116026, China*

[2] *Department of Ocean Engineering, Texas A&M University College, Station 77843, USA*

ARTICLE INFO

Keywords:

Remotely operated underwater vehicles (ROVs)

Trajectory tracking

An adaptive NMPC

Unknown disturbances

Model uncertainties

ABSTRACT

A novel hybrid adaptive control method is presented for trajectory tracking of remotely operated underwater vehicles (ROVs) that addresses unknown disturbances and model uncertainties in this paper. Traditional nonlinear control methods struggle to handle external disturbances and uncertainty in system model. To address the trajectory tracking control needs of ROVs in complex underwater environments, a kinematic and dynamic model is first developed for a fully actuated ROV with six degrees of freedom (6-DOF). The trajectory tracking problem is formulated as an online, nonlinear receding horizon optimization process. Control increments are computed as inputs to this nonlinear optimization problem. An L1 adaptive control method (L1AC) is then developed, incorporating a state observer, adaptive control law, and time filter. The framework retains the rolling optimization process of nonlinear model predictive control (NMPC) while integrating the L1 adaptive component for instant compensation of unknown disturbances and model parameter mismatches. Numerical simulations were conducted to compare the trajectory tracking performance of the proposed hybrid adaptive method with the NMPC method under various disturbances, including ocean currents, waves, random forces, and model uncertainties. The results confirm that the proposed hybrid adaptive control scheme is more effective and robust than the standalone NMPC approach across various scenarios.

1. Introduction

In recent years, there has been a significant increase in the demand for marine resource research, exploration, and development. However, conducting operations in uncharted environments, such as the deep sea, presents substantial safety risks. To mitigate these risks, various underwater vehicles [1,2] are widely utilized in fields like measurement, scientific research, industry, and military applications. As key types of marine robotic systems, they are classified into autonomous underwater vehicles (AUVs) [3,4] and ROVs [5,6] based on their operational method and design. ROVs offer several advantages, including enhanced safety, rapid search capabilities, superior maneuverability, and high modularity. ROVs are widely employed in diverse domains, including territorial exploration, ocean resource extraction, underwater cable installation,

* Corresponding author.

E-mail address: zhangjianing@dlmu.edu.cn

http://dx.doi.org/10.21278/brod76106

Received 12 September 2024; Received in revised form 10 November 2024; Accepted 29 November 2024;

Available online 11 December 2024

ISSN 0007-215X; eISSN 1845-5859

and the maintenance of underwater structures [7-9]. Studies have shown that ROVs, operating without real-time human intervention, can significantly enhance safety and efficiency [10]. However, ROVs typically execute tasks based on control commands transmitted by operators via cables, and those without autonomous control capabilities often show suboptimal performance in specific underwater operations [11]. Controlling ROVs becomes particularly challenging in the presence of external environmental disturbances [12].

To achieve mission objectives, ROVs must be capable of real-time trajectory tracking, obstacle avoidance, and navigation to designated target points [13]. To achieve mission objectives, ROVs must be capable of real-time trajectory tracking, obstacle avoidance, and navigation to designated target points. Various control strategies have been proposed for addressing the trajectory tracking problem of underwater vehicles, including adaptive control [14], PID control [15], sliding mode control (SMC) [16], fuzzy logic control [17,18], neural network control [19], and hybrid control methods [13]. Major challenges for ROVs' automatic control systems include highly nonlinear motion, time-varying hydrodynamic effects, and external environmental disturbances [4, 20]. These challenges create significant difficulties for traditional controllers, which often struggle to manage nonlinear fluid dynamics and external interferences. Therefore, advanced nonlinear control technologies are needed to achieve precise motion control in challenging underwater environments. Compared to traditional nonlinear control techniques, these new methods demand greater robustness. [21] proposed an adaptive system that combines two neural networks, considering nonlinear control inputs, uncertainties in model parameters, and environmental disturbances. This approach has proven to be both effective and robust. However, its reliance on the number of nodes for control performance leads to a heavy computational load. Nonlinear model predictive control (NMPC) [22] is a control technique based on optimization. NMPC offers the advantage of performing rolling optimization of control inputs and planning within the prediction horizon [23], while simultaneously imposing real-time constraints on system states [24]. This capability has made it an essential tool for trajectory tracking of underwater vehicles [25-27]. Molero, et al. [28] proposed an MPC controller to solve the trajectory tracking problem of ROVs. The results showed that this new controller significantly reduced position errors compared to traditional PID controllers. Zhu and Xia [29] developed a novel MPC to address parameter uncertainty in unconstrained discrete linear systems, achieving promising results. Gao, et al. [30] proposed an adaptive positioning control method based on NMPC that integrates the NMPC controller with neural network adaptive control to optimize tracking in a two-dimensional scenario. Long, et al. [31] developed an ESKF-based MPC controller for trajectory tracking control. The robustness of this approach was confirmed through simulation experiments, showing high tracking accuracy. Although NMPC has shown promising results in complex underwater nonlinear environments, there remains significant room for theoretical improvement in managing disturbances. Furthermore, NMPC relies on a highly accurate model to achieve optimal performance, making it difficult to maintain high control precision when model uncertainties exist. This necessitates the development of highly adaptive controllers capable of robustly compensating for unknown model dynamics without relying on prior assumptions. The L1 controller, initially applied in the aerospace field [32,33] , can enhance the performance of existing controllers. By decoupling robustness and adaptivity, it enables fast and robust adaptation of the system under uncertainty and external disturbances [34,35]. Within its control bandwidth, the L1 adaptive controller has a strong capability to suppress interference [36]. It can be directly applied to control a system or used to enhance existing automatic control systems, quickly providing the system with the desired properties through an adaptive reference [37,38]. In the design phase of the control algorithm, once the control flow of the entire system is established, incorporating an L1 controller typically requires minimal adjustment effort [39].

In summary, ROV trajectory tracking control systems require both high precision and robustness. While significant progress has been made in ROV trajectory tracking control, traditional control strategies face challenges in handling nonlinear hydrodynamics and external disturbances, showing limitations in control accuracy and sensitivity to environmental perturbations. Adaptive control and neural network-based methods have shown promise in complex underwater settings, but they heavily depend on computational resources and model parameter accuracy. Although NMPC has become a crucial tool for addressing the trajectory tracking problem due to its optimization capabilities and effective handling of constraints, its performance significantly deteriorates when model uncertainties exist due to its reliance on accurate models. To overcome these

limitations, a novel highly adaptive controller is needed that can robustly compensate for unknown model dynamics without relying on prior assumptions. Such a controller should also seamlessly integrate with existing control frameworks to enhance the system's disturbance rejection capabilities and control accuracy under various environmental conditions.

To tackle these challenges, this study introduces a novel hybrid adaptive controller designed to mitigate disturbances and increase overall control effectiveness. The cost function is formulated in terms of position error, control input, and terminal constraints, converting the trajectory tracking problem into an NMPC problem that is solved through online rolling optimization. To further enhance the adaptability of the NMPC controller and improve trajectory tracking accuracy, an L1 adaptive control component, derived from the ROV's motion model, is integrated. This component is cascaded with the baseline NMPC controller, forming a novel hybrid adaptive control framework. Following the adaptive compensation phase, the updated control input is employed to compute the ROV's state for the next time step. This adaptive approach effectively compensates for model uncertainties and unknown disturbances in complex marine environments while retaining the rolling optimization capabilities of NMPC for precise motion control. The updated pose state is then fed back to the optimizer, triggering a new iteration cycle to maintain the controller's accuracy and robustness. The proposed method is validated through simulations, with results and analyses demonstrating its effectiveness in enhancing the ROV's trajectory tracking performance under various environmental conditions.

The structure of this article is as follows: The first section provides an introduction to the study. The second section derives the detailed mathematical model of the ROV used in this research. Subsequently, the trajectory tracking problem for the ROV is formulated as a rolling optimization control problem using NMPC. To address unknown environmental disturbances and model uncertainty encountered during trajectory tracking, an L1 adaptive augmentation is introduced, forming the theoretical basis for the hybrid adaptive control approach. In the third section, the effectiveness of the proposed hybrid adaptive control method is demonstrated through MATLAB simulations, which highlight the controller's tracking performance. Finally, the fourth section concludes the article by summarizing the proposed control method and the key findings from the simulation results.

2. Mathematical method

2.1 Mathematical model of ROVs

The mathematical modeling of underwater vehicles relies on the hydrodynamic characteristics of rigid bodies and their associated motion behaviors. The study of dynamics is further categorized into kinematics and kinetics [40]. Kinematics focuses on the geometric relationships of position, orientation, and motion paths of moving bodies, while kinetics deals with the forces and torques that induce such motions. By utilizing measured model parameters and hydrodynamic forces, the developed mathematical model can accurately predict the motion of the ROV and can be effectively applied to its control system.

Table 1 Standard symbols for the movement of the ROV

DOF	Force &Moment	Velocities	Position &Euler Angles
Surge	F_{vx}	u	x
Sway	F_{vy}	v	y
Heave	F_{vz}	w	z
Roll	$M_{\omega x}$	p	φ
Pitch	$M_{\omega y}$	q	θ
Yaw	$M_{\omega z}$	r	ψ

In this study, the motion of the ROV is represented using six degrees of freedom, with appropriate coordinate systems established for detailed descriptions. The ROV is modeled as a rigid body within these coordinate systems. For further mathematical formulation, we define the symbolic representations of the ROV's position, orientation, and forces within these coordinate systems to facilitate analysis [4,6], Table 1.

To analyze the motion of the ROV, we define it in two coordinate systems: the Earth-fixed coordinate system and the body-fixed coordinate system. The Earth-fixed coordinate system, also known as the inertial frame, serves as a stationary reference frame relative to the Earth's surface. Conversely, the body-fixed coordinate system is attached to the ROV itself and moves along with it. As illustrated in Fig. 1, the inertial frame is denoted as $O_e(X_e, Y_e, Z_e)$ while the body frame is denoted as $O_b(X_b, Y_b, Z_b)$. These coordinate systems are used to describe the motion of the ROV relative to the inertial reference frame.

Table 2 The 6-DOF motion of the ship is described in vector form

Parameter	Total	Linear	Angular
NEW position	$\boldsymbol{\eta} = [\mathbf{P}, \boldsymbol{\Theta}]^{\mathrm{T}}$	$\mathbf{P} = [\mathbf{x}, \mathbf{y}, \mathbf{z}]^{\mathrm{T}}$	$\boldsymbol{\Theta} = [\mathbf{f}, \boldsymbol{\theta}, \boldsymbol{\psi}]^{\mathrm{T}}$
BODY Velocity	$\mathbf{V} = [\mathbf{v}, \boldsymbol{\omega}]^{\mathrm{T}}$	$\mathbf{v} = [\mathbf{u}, \mathbf{v}, \mathbf{w}]^{\mathrm{T}}$	$\boldsymbol{\omega} = [\mathbf{p}, \mathbf{q}, \mathbf{r}]^{\mathrm{T}}$
BODY force/moment	$\boldsymbol{\tau} = [\boldsymbol{\tau}_1, \boldsymbol{\tau}_2]^{\mathrm{T}}$	$\boldsymbol{\tau}_1 = [\mathbf{F}_{\mathrm{vx}}, \mathbf{F}_{\mathrm{vy}}, \mathbf{F}_{\mathrm{vz}}]^{\mathrm{T}}$	$\boldsymbol{\tau}_2 = [\mathbf{M}_{\omega \mathrm{x}}, \mathbf{M}_{\omega \mathrm{y}}, \mathbf{M}_{\omega \mathrm{z}}]^{\mathrm{T}}$

The position and orientation of the ROV are generally described in an Earth-fixed coordinate system, while its linear and angular velocities are expressed in a body-fixed coordinate system. Standard symbols, as presented in Table 2, are used to denote these quantities. The transformation between these two reference frames is governed by coordinate transformation equations, which are formulated as follows:

$$\dot{\eta} = RV \tag{1}$$

where $\mathbf{R} = \begin{bmatrix} \mathbf{R}_1 & \mathbf{0}_{3\times3} \\ \mathbf{0}_{3\times3} & \mathbf{R}_2 \end{bmatrix}$. Separating the states of angular velocity and linear velocity leads to the following formulations:

$$\dot{P} = R_1 \nu \tag{2}$$

$$\dot{\Theta} = R_2 \omega \tag{3}$$

The rotation matrix that transforms vectors from the body-fixed coordinate system to the inertial frame is given by:

$$\mathbf{R}_1 = \begin{bmatrix} \mathbf{C\psi gC\theta} & \mathbf{-S\psi gCf + C\psi gS\theta gSf} & \mathbf{SfS\psi + C\psi gCfgS\theta} \\ \mathbf{S\psi gC\theta} & \mathbf{C\psi Cf + SfgS\theta gS\psi} & \mathbf{-C\psi gSf + S\theta gS\psi gCf} \\ \mathbf{-S\theta} & \mathbf{C\theta gSf} & \mathbf{C\theta gCf} \end{bmatrix} \tag{4}$$

$$\mathbf{R}_2 = \begin{bmatrix} \mathbf{1} & \mathbf{SfgT\theta} & \mathbf{CfgT\theta} \\ \mathbf{0} & \mathbf{Cf} & \mathbf{-Sf} \\ \mathbf{0} & \mathbf{Sf / C\theta} & \mathbf{Cf / C\theta} \end{bmatrix} \tag{5}$$

where $S\theta$ denotes $\sin\theta$, $C\theta$ denotes $\cos\theta$, and $T\theta$ denotes $\tan\theta$.

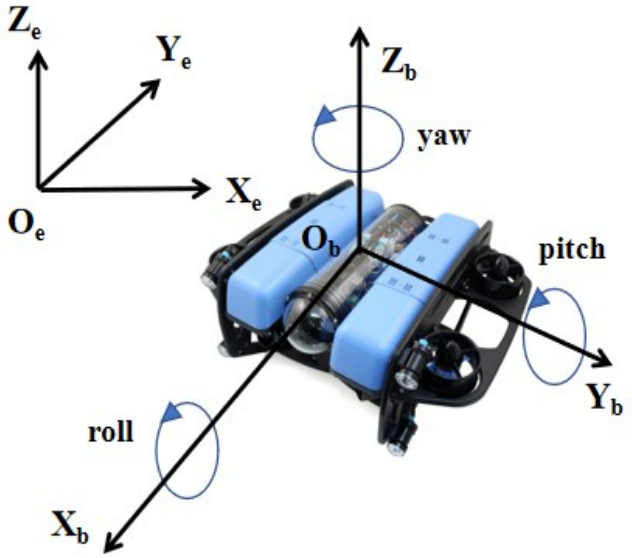

Fig. 1 Reference frames, ROV image courtesy of https://bluerobotics.com

The dynamics of a ROV aim to elucidate the relationship between the forces exerted on the vehicle and its resulting motion. Utilizing the Newton-Euler formulation, the dynamic equations governing an ideal 6-DOF ROV, while neglecting external disturbances and model uncertainties, can be expressed as follows:

$$M\dot{V} + C(V)V + D(V)V + g(\eta) = \tau \tag{6}$$

where τ represents the control input of the system in the absence of disturbances.

$$\begin{aligned} \mathbf{M} &= \mathbf{M}_{\mathbf{RB}} + \mathbf{M}_{\mathbf{A}} = \begin{bmatrix} \mathbf{M}_1 & \mathbf{0}_{3\times3} \\ \mathbf{0}_{3\times3} & \mathbf{J}_1 \end{bmatrix} \\ &= diag(m - X_{\dot{u}}, m - Y_{\dot{v}}, m - Z_{\dot{w}}, I_x - K_{\dot{p}}, I_y - M_{\dot{q}}, I_z - N_{\dot{r}}) \end{aligned} \tag{7}$$

where M_{RB} is the rigid body inertia matrix of the ROV. M_A is the added mass matrix of the vehicle. Given the assumption regarding the center of buoyancy and the specific motion characteristics of the ROV considered in this study, the contribution of the non-diagonal elements is neglected. $C(V)$ is the Coriolis and centripetal force, including the rigid-body Coriolis force term (C_{RB}) and hydrodynamic Coriolis force term (C_A). According to literature [41], the following expression is obtained through Lagrangian parameterization method:

$$\mathbf{C(V)}=\begin{bmatrix}\mathbf{0}_{3\times3} & \mathbf{C_1(V)}\\ \mathbf{C_2(V)} & \end{bmatrix}$$

$$=\begin{bmatrix}
\mathbf{0} & \mathbf{0} & \mathbf{0} & \mathbf{0} & \mathbf{Z_{wz}.w+mw} & \mathbf{-mv}\\
\mathbf{0} & \mathbf{0} & \mathbf{0} & \mathbf{-Z_{wz}.w-mw} & \mathbf{0} & \mathbf{mu-X_{ux}.u}\\
\mathbf{0} & \mathbf{0} & \mathbf{0} & \mathbf{mv-Y_{vy}.v} & \mathbf{X_{ux}.u-mu} & \mathbf{0}\\
\mathbf{0} & \mathbf{mw-Z_{wz}.w} & \mathbf{Y_{vy}.v-mw} & \mathbf{0} & \mathbf{I_zr-N_{rn}.r} & \mathbf{M_{qm}.q-I_yq}\\
\mathbf{Z_{wz}.w-mw} & \mathbf{0} & \mathbf{-X_{ux}.u-mu} & \mathbf{N_r.r-I_zr} & \mathbf{0} & \mathbf{I_xp-K_{pk}.p}\\
\mathbf{mv-Y_{vy}.v} & \mathbf{X_{ux}.u-mu} & \mathbf{0} & \mathbf{I_yq-M_{qm}.q} & \mathbf{K_{pk}.p-I_xp} & \mathbf{0}
\end{bmatrix} \tag{8}$$

In general, $D(V)$ is the approximate damping term that accounts for both linear and quadratic resistances, and it can be expressed as follows:

$$\begin{aligned}&\mathbf{D(V)}=\begin{bmatrix}\mathbf{D_1(V)} & \mathbf{0}_{3\times3}\\ \mathbf{0}_{3\times3} & \mathbf{D_2(V)}\end{bmatrix}\\ &=\mathrm{diag}(-X_{ux}-X_{ux|ux|}\,|u|,\quad -Y_{vy}-Y_{vy|vy|}\,|v|,\quad -Z_{wz}-Z_{wz|wz|}\,|w|,\\ &-K_{pk}-K_{pk|pk|}\,|p|,\quad -M_{qm}-M_{qm|qm|}\,|q|,\quad -N_{rn}-N_{rn|rn|}\,|r|)\end{aligned} \tag{9}$$

where $g(\eta)$ represents the static water restoring force, and it is assumed that the buoyancy force is equal to the gravitational force, denoted as $B=mg$, where g is the gravitational acceleration. Additionally, it is assumed that (x_b, y_b, z_b) represents the coordinates of the center of buoyancy of the ROV in the body frame.

$$\mathbf{g(\eta)}=\begin{bmatrix}\mathbf{g_1(\eta)}\\ \mathbf{g_2(\eta)}\end{bmatrix}=\begin{bmatrix}
\mathbf{(mg-B)\sin\theta}\\
\mathbf{-(mg-B)\cos\theta\sin\varphi}\\
\mathbf{-(mg-B)\cos\theta\cos\varphi}\\
\mathbf{y_bB\cos\theta\cos\varphi-z_bB\cos\theta\sin\varphi}\\
\mathbf{-z_bB\sin\theta-x_bB\cos\theta\cos\varphi}\\
\mathbf{x_bB\cos\theta\sin\varphi+y_bB\sin\theta}
\end{bmatrix} \tag{10}$$

The equation above represents the dynamics of an ROV in an ideal state, neglecting external environmental disturbances. The derived result is similar to that presented in [37]. This equation can be rewritten as follows:

$$\dot{V}=-M^{-1}[C(V)+D(V)]V+M^{-1}\tau \tag{11}$$

The time step is Δt discrete time, and the fourth-order explicit Runge-Kutta method is used to represent the state information of ROV in the $k+1$ time step:

$$X(k+1)=f_{RK4}(X(k),\tau(k),\Delta t) \tag{12}$$

where $X=[\eta,V]^T$ is the status information of ROV.

2.2 NMPC formulation

NMPC is a control strategy that relies on numerical optimization techniques. It incorporates a nonlinear system model, a predefined cost function, and a numerical optimization solver. By iteratively minimizing the cost function, NMPC optimizes the control inputs to the system model, thereby predicting future control actions and system responses. Within each prediction horizon, the NMPC controller computes an optimal sequence of future control inputs but only implements the first control input in real-time. This receding horizon strategy enables the nonlinear system's response to converge towards a desired reference trajectory. When external disturbances are neglected, the system dynamics are expressed in the following compact mathematical form:

$$\dot{\mathbf{X}}=\begin{bmatrix}\dot{\boldsymbol{\eta}}\\ \dot{\mathbf{V}}\end{bmatrix}=\begin{bmatrix}\mathbf{RV}\\ \mathbf{-M^{-1}[C(V)+D(V)]\ V-M^{-1}g(\eta)+M^{-1}\tau_b}\end{bmatrix} \tag{13}$$

where τ_b represents the input of the baseline controller in the absence of disturbances.

As a predictive model, the aforementioned equation does not account for external environmental disturbances or system uncertainties. Since model parameter uncertainties must be considered in the study, an uncertainty coefficient will be introduced in subsequent analysis.

The cost function ($J(X,\tau)$) is formulated based on the deviation between the predicted system response and the desired system output, as well as the magnitude of the control inputs. The objective is to minimize this cost function to reduce both the tracking error and the control effort. This approach determines the optimal control inputs that satisfy the constraints over the next N time steps. Subsequently, only the first control input from this sequence is applied to the system. The desired navigation trajectory and state information $X_R(x_R,y_R,z_R)$ for the ROV are assumed to be known in advance, smooth, and bounded. The structure of the predefined cost function at time step k is given as follows:

$$J(X_n,\tau_b(\cdot\,|\,k))=\sum_{n=0}^{N-1}L_1(X(n\,|\,k),\tau_b(n\,|\,k))+L_2(X(N\,|\,k)) \tag{14}$$

In this context, $L_1(X,\tau_b)$ is defined as the stage cost:

$$L_1(X,\tau_b)=\|X-X_R\|_{Q_1}^2+\|\tau_b\|_{Q_2}^2 \tag{15}$$

$L_2(X)$ is the terminal constraint cost:

$$L_2(X)=\|X-X_R\|_{Q_3}^2 \tag{16}$$

where $Q_1,Q_2\in R^{6\times6}$ is a positive definite matrix that consists of two weight matrices that can be set independently. Their main role is to adjust the weight ratio of position error and input during the optimization process. In this paper, given the consideration of position error and the requirement for input (to minimize energy consumption as much as possible), a larger value is chosen for Q_2. The positive definite matrix $Q_3\in R^{6\times6}$ is the solution to the Lyapunov equation [42].

To solve the optimization problem in the code, numerical computation is employed. The entire solution process involves discretizing the cost function over the prediction time horizon and summing it up. The prediction time domain is uniformly divided into N nodes, and the cost function is evaluated at each time node.

At time step k, the optimization problem concerning the aircraft state X and input τ is solved in the prediction horizon, incorporating the cost function J. The optimization problem can be described as follows:

$$\min_{u(\cdot|k)} J(X_n, \tau_b(\cdot|k)) = \sum_{n=0}^{N-1} L_1(X(n|k), \tau_b(n|k)) + L_2(X(N|k)) \tag{17a}$$

$$s.t. X(n+1|k) = f_{RK4}(X(n|k), \tau_b(n|k)) \tag{17b}$$

$$\begin{aligned} &X_{\min} \le X(n|k) \le X_{\max}, \tau_{\min} \le \tau_b(n|k) \le \tau_{\max}, \mathrm{n} \in \{0, \cdots, N-1\} \\ &\tau_b(n|k) \in U, X(n|k) \in X_f \end{aligned} \tag{17c}$$

$$X(0|k) = X(k) \tag{17d}$$

where $X_{\min}, X_{\max}$ and $\tau_{\min}, \tau_{\max}$ are vehicle state and control inputs constraints. The fourth-order Runge-Kutta method is utilized to solve the optimization problem, providing a numerical solution for the system's dynamic equations at each time step.

By successfully solving eq. (17), the optimal state trajectory and inputs $(X^*(\bullet|k), \tau_b^*(\bullet|k))$ can be obtained. Then, the NMPC control action applied to the system at time step k is defined as:

$$\tau_b(X_k) = \tau_b^*(0|k) \tag{18}$$

Ultimately, the nominal closed-loop system can be expressed in the following form:

$$X_{k+1} = f_{RK4}(X_k, \tau_b(X_k)) \tag{19}$$

Next, we summarize the fundamental assumptions of NMPC principles to establish the sufficient conditions for the stability of the nominal closed-loop system.

Assumption 1: Considering the closed terminal set X_f related to eq. (17) and the terminal cost $L_2(X)$ from eq. (16), we assume that for each state $X_k \in X_f$, there exists an acceptable control value $\tau_{loc}(X_k) \in U$ at any time step k such that the following two conditions hold:

$$X_{k+1} = f_{RK4}(X_k, \tau_{loc}(X_k)) \in X_f \tag{20}$$

$$L_2(X_{k+1}) + L_2(X_k, \tau_{loc}(X_k)) \le L_2(X_k) \tag{21}$$

Theorem 1: If Assumption 1 holds, then under the feedback law $\tau_b(X_k)$ in eq (17a-d), the nominal closed-loop system $X_{k+1} = f_{RK4}(X_k, \tau(X_k))$ achieves recursive feasibility and asymptotic stability [43].

Through internal optimization, the optimal solution of the cost function is continuously sought within the prediction time interval, allowing for the determination of the required input sequence for the next time step. This process is repeated iteratively, achieving the objective of rolling optimization. The nonlinear optimization process described above generates the system input τ_b for the baseline controller, which is

subsequently used as an input to the cascade L1 adaptive augmentation for further computation in the next step.

2.3 L1 adaptive augmentation

In real-world scenarios, developing accurate models is particularly challenging, especially in complex underwater environments where the motion of ROVs is affected by uncertainties and disturbances, such as varying propeller dynamics and wind waves. The previously derived NMPC control model assumes an idealized description of ROV motion, which does not account for these complexities. To address this, the actual system uncertainties and unknown external disturbances are incorporated into the state-space representation of the system. Specifically, we directly consider the uncertainties in thrust and torque across all six degrees of freedom and introduce external disturbances affecting thrust and torque for each degree of freedom:

$$M\dot{V}+C(V)V+D(V)V+g(\eta)=\tau_b+\sigma_m \tag{22}$$

In this study, $\boldsymbol{\sigma_m(t)=[\varsigma,\zeta]^T}$ represents unknown external disturbances, where $\boldsymbol{\varsigma=[\varsigma_x,\varsigma_y,\varsigma_z]^T}$ denotes disturbances affecting linear acceleration, and $\boldsymbol{\zeta=[\zeta_x,\zeta_y,\zeta_z]^T}$ signifies environmental disturbances influencing angular acceleration. The ROV considered in this study is a fully actuated system, capable of providing linear acceleration along all three coordinate axes and angular acceleration about all three coordinate axes. To address the uncertainties in the actual system and unknown external disturbances, the L1AC approach is employed. The L1AC framework consists of a state predictor, an adaptive law, and a low-pass filter (LPF) [39], as depicted in Fig. 2. The state predictor replicates the system dynamics, replacing unknown uncertainties with estimated values. The output of the L1AC is then applied to the uncertain dynamic equation:

$$M\dot{V}+C(V)V+D(V)V+g(\eta)=\tau_b(t)+\tau_{L1}(t)+\sigma_m(t,V(t)) \tag{23}$$

where $\tau_{L1}(t)\in R^{6\times1}$ represents the compensation values generated by the L1 control for cascading purposes. The predictor in the L1 Adaptive Control (L1AC) framework is formulated as follows:

$$\dot{\hat{V}}(t)=-M^{-1}[C(V)+D(V)]V-M^{-1}g(\eta)+M^{-1}[\tau_b(t)+\tau_{L1}(t)+\hat{\sigma}_m(t,V(t))]+A_s\tilde{V}(t) \tag{24}$$

where $\tilde{V}(t)=\hat{V}(t)-V(t)$ denotes the state error, while $A_s\in R^{6\times6}$ is an adjustable diagonal Hurwitz matrix. The L1 Adaptive Control (L1AC) is implemented using a nonlinear reference model, which employs a piecewise constant adaptive law [36,38] to estimate the matched uncertainties. The piecewise constant adaptive rate is applied to $t\in[k\Delta t,(k+1)\Delta t)$:

$$\hat{\sigma}_m(t)=\hat{\sigma}_m(k\Delta t)=-\bar{B}(k\Delta t)^{-1}\Phi^{-1}\mu(k\Delta t) \tag{25}$$

where Δt represents the time step, and $\bar{B}$ is an invertible square matrix:

$$\bar{B}(k\Delta t)=-M(k\Delta t)^{-1} \tag{26}$$

$$\Phi = A_s^{-1}(\exp(A_s \Delta t) - I) \tag{27}$$

For $k \in N$:

$$\mu(k\Delta t) = \exp(A_s \Delta t)\tilde{V}(k\Delta t) \tag{28}$$

Next, we define a first-order continuous-time filter $C(s)$ [44]. The L1AC control law is:

$$\tau_{L1}(s) = -C(s)\hat{\sigma}_m(s) \tag{29}$$

In practical discrete-time implementation, the control rate at the $k-th$ time step can be defined as follows:

$$\tau_{L1,k} = \hat{\sigma}_{m,k}\, \omega_{co}\Delta t + \tau_{L1,k-1}(1-\omega_{co}\Delta t) \tag{30}$$

where ω_{co} represents the frequency limit of a suitably chosen first-order filter. The L1AC observer in discrete time evolves as follows:

$$\hat{V}_{k+1} = \hat{V}_k + [-M_k^{-1}(C(V_k) + D(V_k))V_k - M_k^{-1}g(\eta) + M_k^{-1}(\tau_{b,k} + \tau_{L1,k} + \hat{\sigma}_{m,k}) + A_s\tilde{V}_k]\Delta t \tag{31}$$

The piecewise constant adaptive law can compensate for the state prediction error at the subsequent sampling time $(k+1)\Delta t$:

$$\dot{\tilde{V}}(t) = A_s\tilde{V}(t) + \bar{B}(t)(\hat{\sigma}_m(t) - \sigma_m(t)) \tag{32}$$

For complete proofs of stability and performance of L1 adaptive controller refer to [45].

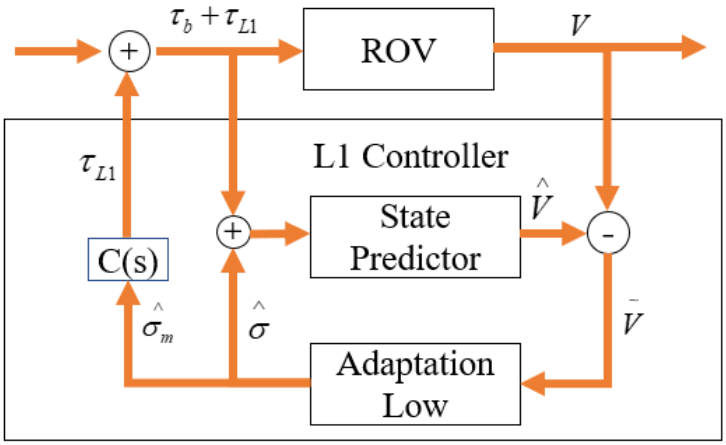

Fig.2 L1AC framework schematic diagram

Based on the above formula, the components of the L1AC framework are illustrated in the Fig.2, consisting of three parts: a LPF, a state predictor, and an adaptive law.

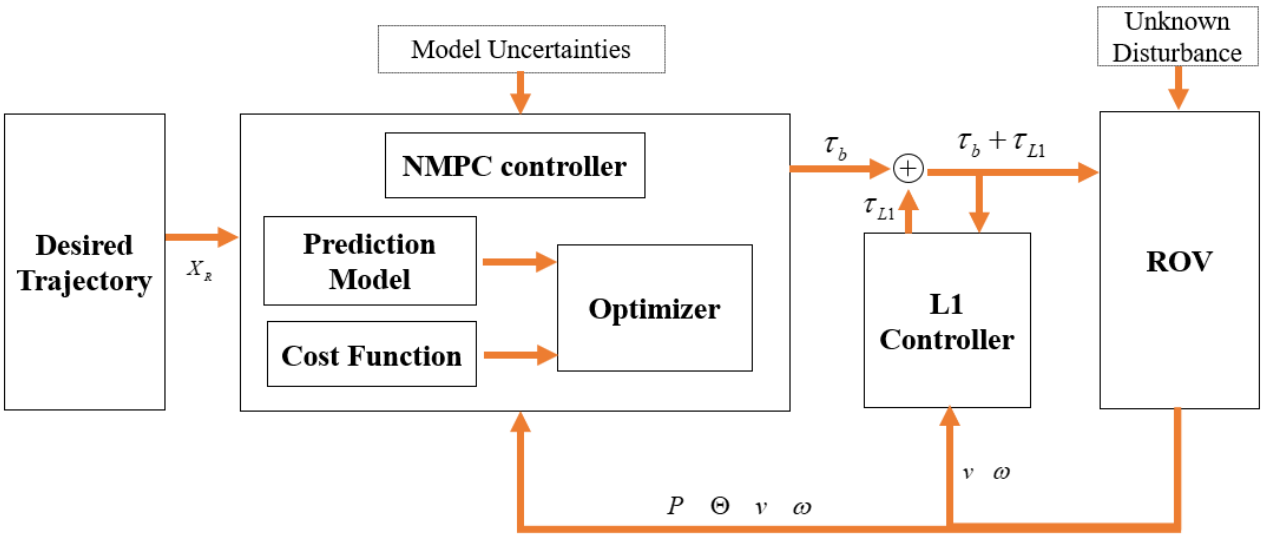

Fig.3 Structure diagram of hybrid adaptive controller

The Fig.3 presents a schematic diagram of the entire controller structure. In this study, two types of disturbances are considered: unknown environmental disturbances directly acting on the ROV body and model uncertainties affecting the baseline controller. The initial control inputs are computed by the NMPC controller to obtain the baseline control input (τ_b). This input (τ_b) is then fed into the adaptive control module to perform disturbance compensation. Consequently, the combined adaptive control input is generated and applied to the ROV model to compute the pose state, which is subsequently provided to the controller for the next iteration.

2.4 Algorithm

The calculation program of the newly proposed hybrid adaptive control framework is as follows:

Algorithm L1+NMPC Trajectory Tracking Algorithm

Input: $X(0)$ (initial state), X_R (desired trajectory), Δt (time step), T (simulation time), Q_1, Q_2 (weighting matrices), $\tau_{\min}, \tau_{\max}$ (input constrains), A_s, ω_{co} (L1 parameters)

1: $k \leftarrow 1$

2: $X(k) \leftarrow X(0)$

3: While $k \times \Delta t \le T$ do

4: Construct NMPC problem with $X(0)$ using eq. (16) and (17).

Compute $\tau_b(k)$.

5: Construct L1AC with $\tau_b(k)$.

Compute $\hat{V}, \tilde{V}, \hat{\sigma}, \bar{B}, \Phi, \mu(k\Delta t)$ using eq. (24-28) and (32).

Compute $\tau_{L1}(k)$ using eq. (31) and update $\tau(k) = \tau_{L1}(k) + \tau_b(k)$.

6: Implement $\tau(k)$ to the ROV with disturbances.

7: Compute the current state $X(k+1)$ using eq. (12).

8: $k \leftarrow k+1$

9: End while.

3. Simulation study

3.1 Parameter and operating condition setting

The three-dimensional sinusoidal reference trajectory used in the numerical simulations is defined as follows:

$$\begin{cases} x_R = 0.5*t \\ y_R = 0.5*t \\ z_R = 10*\sin(0.1*t) \end{cases} \tag{33}$$

The three-dimensional helical reference trajectory is defined as:

$$\begin{cases} x_R = t \\ y_R = 10*\sin(0.1*t) \\ z_R = 10*\cos(0.1*t) \end{cases} \tag{34}$$

The key specifications of the ROV utilized in the simulations are presented in Table 3 and are derived from [46].

This study uses the BlueROV2 platform to perform numerical simulations for validating control algorithms. The ROV has dimensions of 457 mm in length, 338 mm in width, and 254 mm in height. It employs vectored thrust propulsion and is equipped with eight thrusters, allowing for control with six degrees of freedom. The maximum diving depth of the ROV is 100 m, and it can reach a forward speed of up to 1.5 m/s.

Table 3 Parameter values of the BlueROV2

Parameter	Value	Unit	Parameter	Value	Unit
m	11.5	kg	$K_{\dot{pk}}$	-0.12	kgm^2
I_x	0.16	kgm^2	$M_{\dot{qm}}$	-0.12	kgm^2
I_y	0.16	kgm^2	$N_{\dot{rn}}$	-0.12	kgm^2
I_z	0.16	kgm^2	X_{ux}	-4.03	kg/s
$X_{\dot{ux}}$	-5.5	kg	Y_{vy}	-6.22	kg/s
$Y_{\dot{vy}}$	-12.7	kg	Z_{wz}	-5.18	kg/s
$Z_{\dot{wz}}$	-14.57	kg	$Y_{\|vy\|vy}$	21.66	kg/m
g	9.81	m/s^2	$Z_{\|wz\|wz}$	36.99	kg/m
$X_{\|ux\|ux}$	-18.18	kg/m	$K_{\|pk\|pk}$	-1.55	kgm^2/rad^2
$M_{\|qm\|qm}$	-1.55	kgm^2/rad^2	$N_{\|rn\|rn}$	-1.55	kgm^2/rad^2
K_{pk}	-0.07	kgm^2/(s.rad)	M_{qm}	-0.07	kgm^2/(s.rad)
N_{rn}	-0.07	kgm^2/(s.rad)			

The initial setup conditions for the numerical simulation are as follows: the initial velocity state ($\mathbf{v_0} = \mathbf{[0,0,0,0,0,0]^T}$) vector's first three components are given in meters per second (m/s), while the remaining three are in radians per second (rad/s). The prediction time horizon is denoted as $N = 5$, and the sampling period is specified. The control input constraints for the NMPC are also defined:

$$\boldsymbol{\tau}_{\max} = \left[\mathbf{50},\ \mathbf{50},\ \mathbf{50},\ \mathbf{50},\ \mathbf{50},\ \mathbf{50}\right]^{\mathbf{T}} \tag{35}$$

$$\boldsymbol{\tau}_{\min} = \left[\mathbf{-50},\ \mathbf{-50},\ \mathbf{-50},\ \mathbf{-50},\ \mathbf{-50},\ \mathbf{-50}\right]^{\mathbf{T}} \tag{36}$$

NMPC position error weight matrix:

$$\mathbf{Q_1} = \mathbf{20} \times \mathbf{diag(1,1,1,1,1,1)} \tag{37}$$

Input value weight matrix:

$$\mathbf{Q_2} = \mathbf{20} \times \mathbf{diag(1,1,1,1,1,1)} \tag{38}$$

All simulations were conducted on a laptop equipped with an Intel Core i7-10750H CPU @ 2.60GHz dual-core processor, using a simulator based on MATLAB R2018b. Two reference trajectories were chosen for the simulations, which were performed under both undisturbed conditions and with ocean disturbances. The initial pose state of the ROV for the sine curve trajectory tracking simulation is defined as $\boldsymbol{\eta_0} = \mathbf{[1m,1m,1m,0rad,0rad,0rad]^T}$, while the initial pose state for the helix curve trajectory tracking simulation is defined as $\boldsymbol{\eta_0} = \mathbf{[1m,1m,9m,0rad,0rad,0rad]^T}$. In designing the simulation experiments, four types of disturbances were considered: no disturbance, ocean current disturbance, random disturbance, wave disturbance, and model uncertainties due to inaccurate coefficients in the NMPC dynamic model. The coefficients for the L1 controller are set to $\boldsymbol{\omega_{co}} = \mathbf{[2,2,2,2,2,2]^T}$, where the six vector values are in rad/s, and $\mathbf{A_s} = \mathbf{-diag[5,5,5,10,10,10]^T}$ is an adjustable diagonal Hurwitz matrix. The above interferences were applied in the form of fluid velocity.

The random disturbance:

$$\begin{cases} v_x = 0.1 * rand(1)\, m/s \\ v_y = 0.3 * rand(1)\, m/s \\ v_z = 0.4 * rand(1)\, m/s \end{cases} \tag{39}$$

The ocean current disturbance:

$$\begin{cases} v_x = 0.3\, m/s \\ v_y = 0.1\, m/s \\ v_z = 0.1\, m/s \end{cases} \tag{40}$$

The wave disturbance:

$$\begin{cases} v_x = 0.2\sin(5t) + 0.1\sin(10t)\, m/s \\ v_y = 0.1\sin(5t) + 0.1\sin(5t)\, m/s \\ v_z = 0.1\sin(5t)\, m/s \end{cases} \tag{41}$$

The fourth operating condition is model parameter uncertainty, where errors exist in the control model parameters within the NMPC. This study considers a 20% uncertainty in the ROV model parameters to evaluate its impact on the controller's performance.

Numerical simulation experiments were conducted to assess the performance of both the basic NMPC controller and the proposed hybrid adaptive controller for trajectory tracking under four distinct operating conditions, as well as an unperturbed scenario. The results of these experiments are summarized below.

3.2 Simulation results analysis

3.2.1 Sine curve motion trajectory

Numerical simulation experiments were conducted to evaluate the performance of the basic NMPC controller and the proposed hybrid adaptive controller for trajectory tracking control under four distinct operating conditions and unperturbed scenarios. The results of these experiments are presented below.

As illustrated in Fig. 4, the orange curve represents the simulation results without any disturbance, the green curve shows results under ocean current disturbance, the purple curve corresponds to random disturbance, the blue curve depicts results with wave disturbance, and the red curve indicates results with model parameter uncertainty. The black curve represents the reference trajectory. The ROV successfully performs real-time tracking of the desired trajectory under the influence of both controllers across different conditions. These results demonstrate the convergence and stability of the hybrid control algorithm.

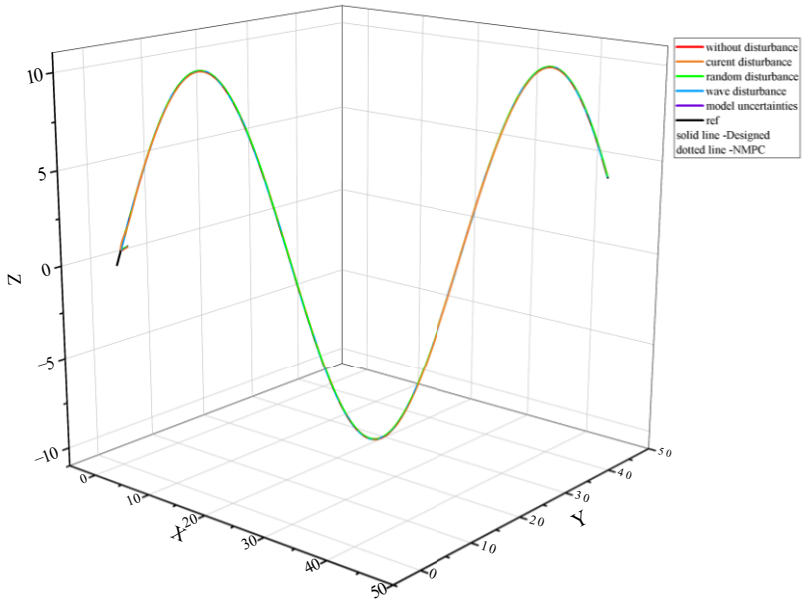

Fig.4 Trajectory tracking results of three-dimensional sine curve under different operating conditions

Fig. 5 presents the time history curves of the ROV's trajectory tracking results in three directions. The following key observations can be made:

(1) Across all simulations, despite initial tracking errors, the ROV under both controllers effectively follows the desired trajectory.

(2) While the presence of disturbances affects the ROV's tracking performance, the controller consistently adjusts the trajectory back to the desired path. The position tracking errors of both controllers remain bounded, demonstrating the effectiveness of the designed controller in trajectory tracking.

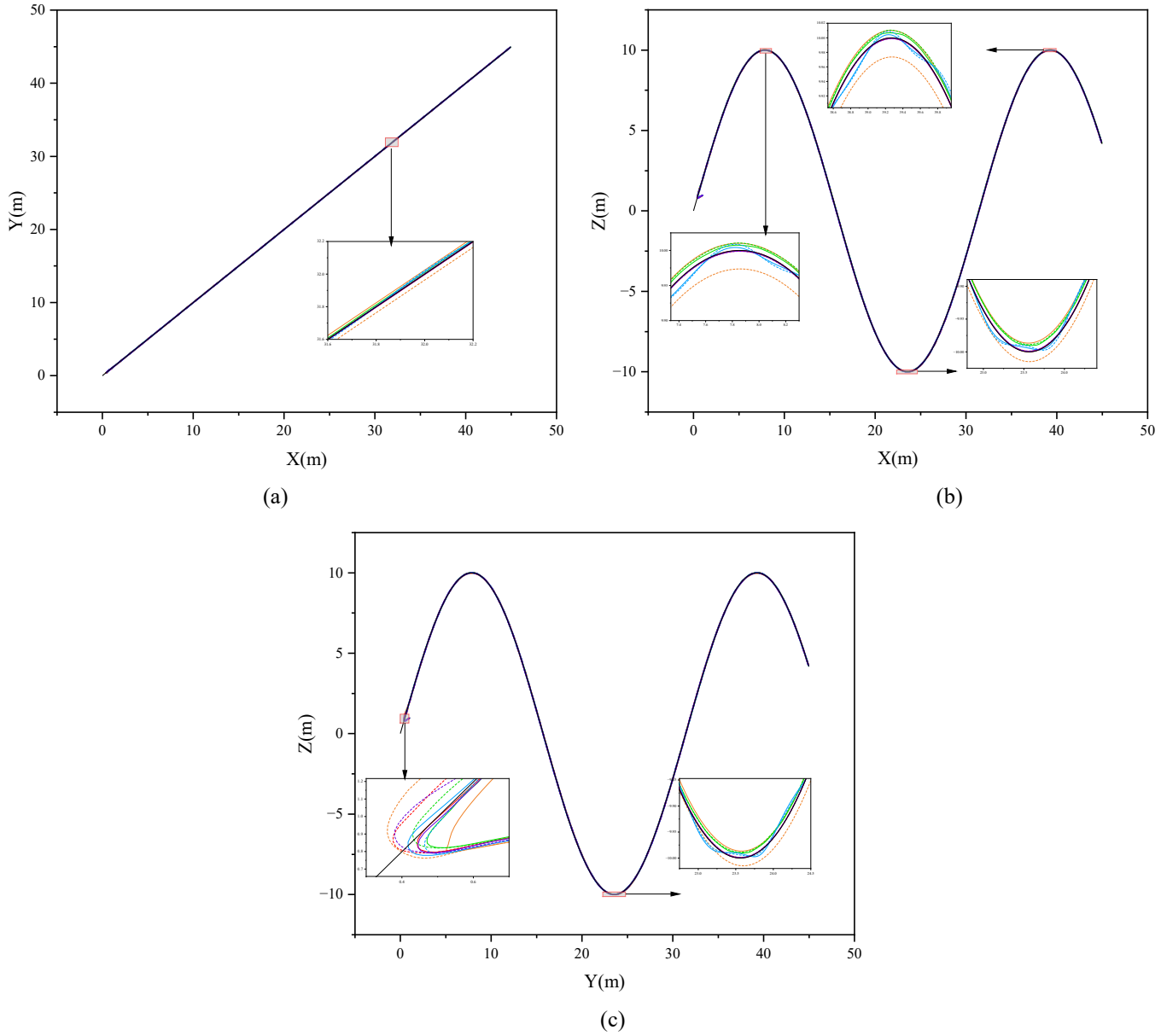

Fig.5 Time history curves of ROV trajectory tracking results on various degrees of freedom

Further insights can be drawn from the detailed local enlarged views in Fig. 5:

(1) After the initial phase, the solid line representing the designed controller remains consistently closer to the reference trajectory than the NMPC controller, indicating superior tracking performance of the designed controller.

(2) As seen in the enlarged view of the initial point in Fig. 5(b), due to the adaptive component of the designed controller, an overshoot occurs when the ROV quickly approaches the desired trajectory near the initial point. At this moment, the solid line representing the designed controller deviates further from the desired trajectory. However, it rapidly converges back to the desired trajectory, achieving more accurate tracking in a short time.

(3) A relatively gradual rate of trajectory change leads to better tracking performance, as observed in the straight-line sections in Fig. 5(a). However, position errors significantly increase at turning points, as

shown in the local magnified view in Fig. 5(c). Regardless of whether at turning points or where the trajectory slope is more gradual, the designed controller consistently exhibits higher tracking accuracy.

The primary metric for evaluating tracking performance in this study is the position tracking error, defined as:

$$e=\sqrt{(x-x_R)^2+(y-y_R)^2+(z-z_R)^2} \tag{42}$$

where (x,y,z) represent the actual position and (x_R,y_R,z_R) represent the desired position.

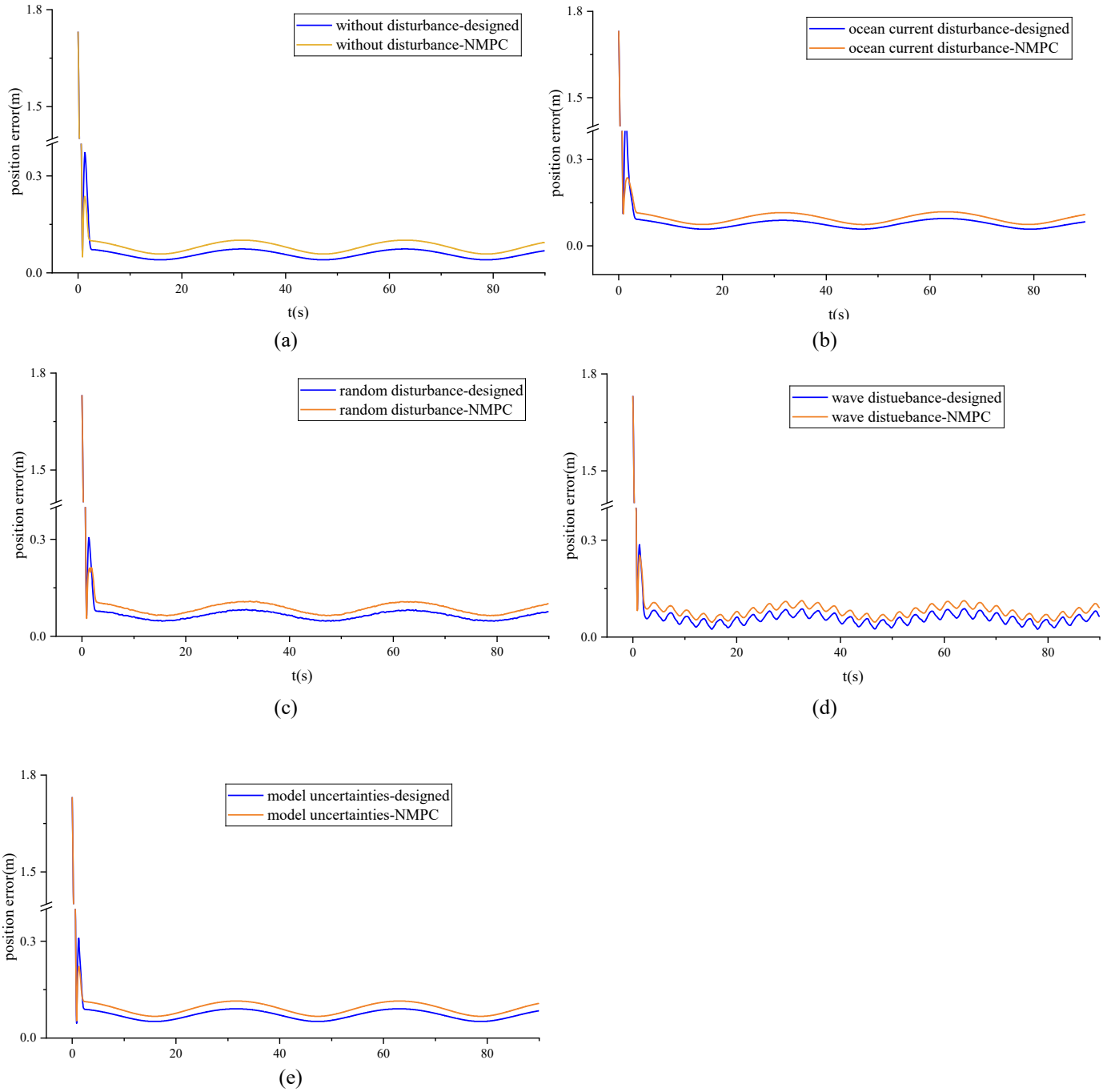

Fig.6 The time history curve of trajectory error value under different disturbances

The time history curve of the trajectory error under different disturbances (Fig. 6) provides a more intuitive and quantitative comparison of the trajectory tracking performance of the two controllers. In the initial phase, due to a large initial position error, the time history curves for the position errors of both

controllers exhibit significant variations. Notably, the error for the hybrid controller initially increases sharply and is larger than that of the NMPC controller. This is attributed to the control overshoot caused by the adaptive component of the designed controller, which aligns with our earlier observations of the position time history curve. After the ROV approaches the reference trajectory, the error curves under all conditions become smoother, with no significant jitter, which is beneficial for ROV control and confirms the stability and convergence of the controller.

The time history curve of the position error also shows periodic variations, corresponding to the periodic nature of the sinusoidal reference trajectory. Across all conditions, the tracking error of the new hybrid adaptive controller is significantly smaller than that of the basic NMPC controller. The designed controller substantially reduces the tracking position error compared to the NMPC controller, fully verifying the superior performance of the proposed controller in terms of trajectory tracking accuracy.

The data indicates that the average error for both ROV controllers under normal (undisturbed) conditions is relatively low. As illustrated in Fig. 7, the introduction of environmental disturbances and model errors significantly increases the average position tracking error. Although the NMPC controller can effectively track the desired trajectory, its performance is considerably affected by disturbances. When the L1 controller is cascaded to form a hybrid adaptive controller, the average position errors under the same four disturbances are reduced.

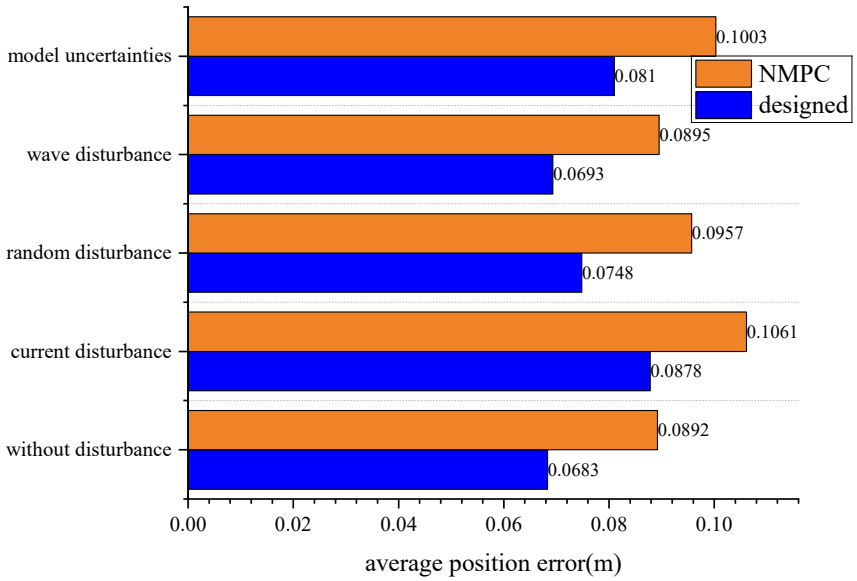

Fig.7 Comparison of tracking error with various uncertainties between the NMPC and the L1+NMPC enhancement

Further analysis of the data reveals that the hybrid adaptive controller outperforms the baseline NMPC controller in reducing position tracking errors across various experimental conditions. Specifically, the adaptive hybrid controller reduces the position tracking error by 23.4% under undisturbed conditions, 17.2% under ocean current disturbances, 21.8% under random disturbances, 22.6% under wave disturbances, and 19.2% under model uncertainties. Although the basic NMPC controller shows favorable position tracking accuracy, its performance heavily depends on the availability of an accurate dynamic model. In contrast, the proposed hybrid controller demonstrates superior tracking accuracy, even when model parameters are set to 80% of their true values, outperforming the NMPC controller's tracking accuracy under undisturbed conditions. The robustness and adaptability of the hybrid controller in the presence of disturbances affirm the efficacy of the proposed method.

As illustrated in Fig. 8, under the initial large position error, the controller output reaches a saturated high value to try to quickly correct the position. Under disturbed conditions, the output forces and torques exhibit significant fluctuations due to the ROV's deviation from the reference trajectory caused by environmental disturbances. These disturbances necessitate rapid adjustments in control forces and torques to realign the ROV with the desired trajectory.

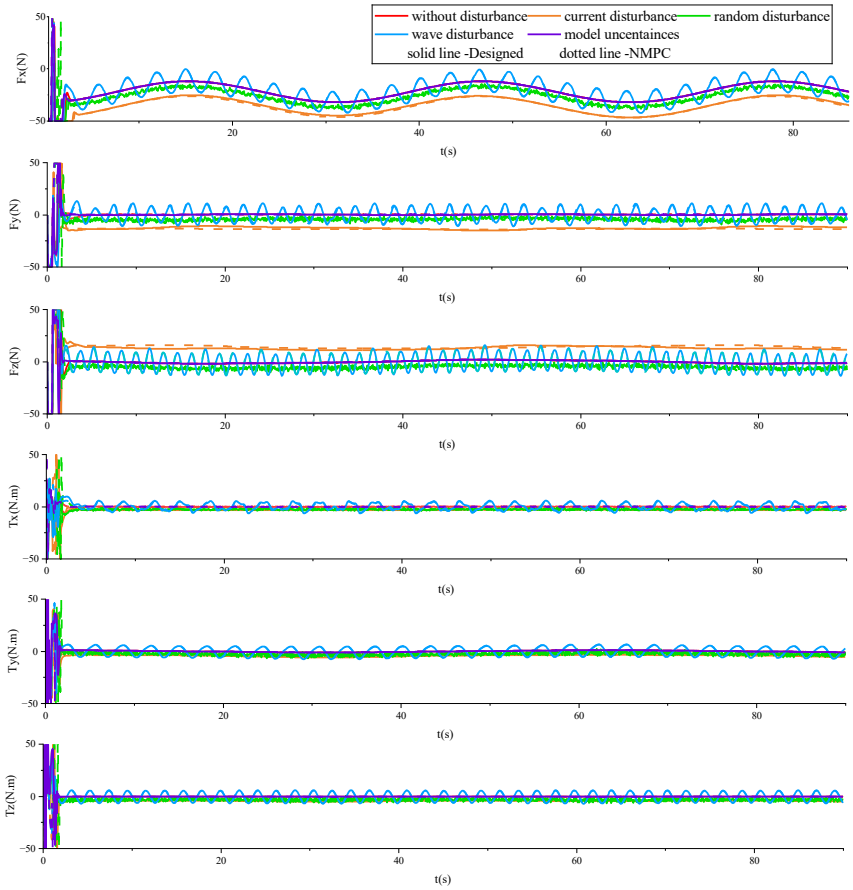

Fig.8 The designed control & NMPC actual output force and torque time history diagram

Comparatively, under the same conditions, the actual control inputs calculated by both the NMPC and the hybrid adaptive controller are closely aligned. This indicates that both controllers effectively reduce position error while maintaining control forces and torques with minimal jitter, reflecting overall stability. The calculated thrust outputs based on these optimal control inputs are facilitating efficient thruster control and aligning with the operational characteristics of marine vehicle thrusters. This further confirms the stability and effectiveness of the designed controller.

3.2.2 Spiral motion trajectory

From the above simulations, it can be concluded that the effectiveness of trajectory tracking is significantly influenced by the curvature changes of the preset trajectory. In practical engineering applications, ROVs often encounter a variety of trajectory types. Therefore, a spiral trajectory is selected for simulation to better represent and address the complexities involved in real-world scenarios.

In the simulation of spiral trajectory tracking, the ROV encounters curves with varying curvatures in all directions. The simulation results are depicted in Fig. 9. As illustrated in Fig. 10, it is evident that during the spiral trajectory tracking process, the tracking accuracy of the designed hybrid controller surpasses that of the NMPC controller, with the trajectory following the reference path more closely. This outcome confirms the effectiveness of the proposed method.

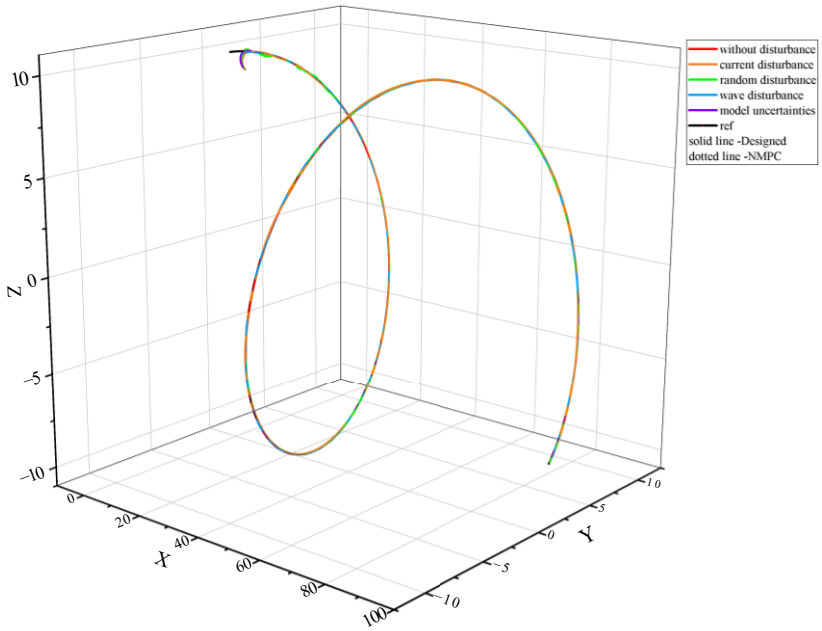

Fig.9 Trajectory tracking results of three-dimensional helix curve under different operating conditions

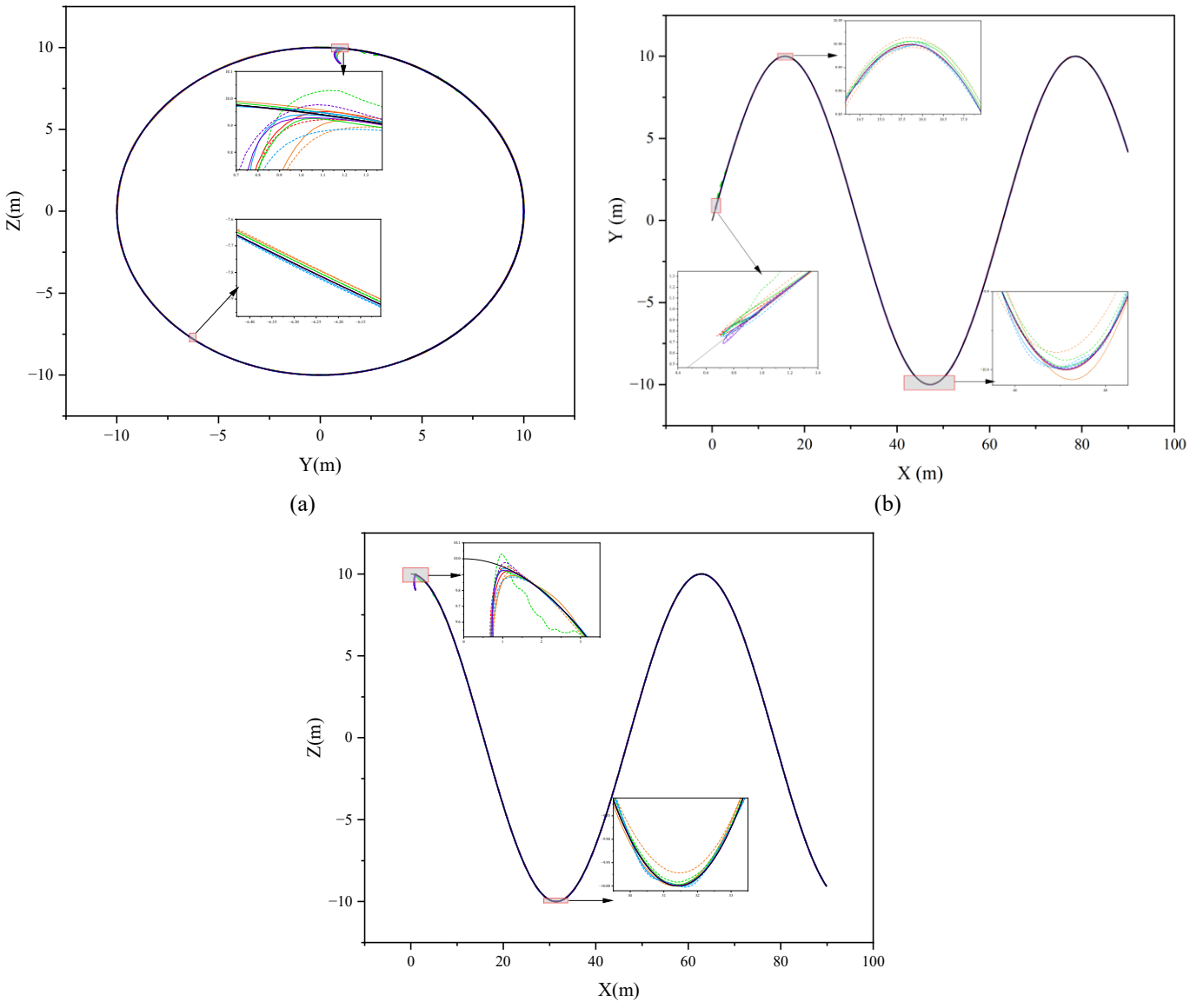

Fig.10 Time history curves of ROV trajectory tracking errors on various degrees of freedom

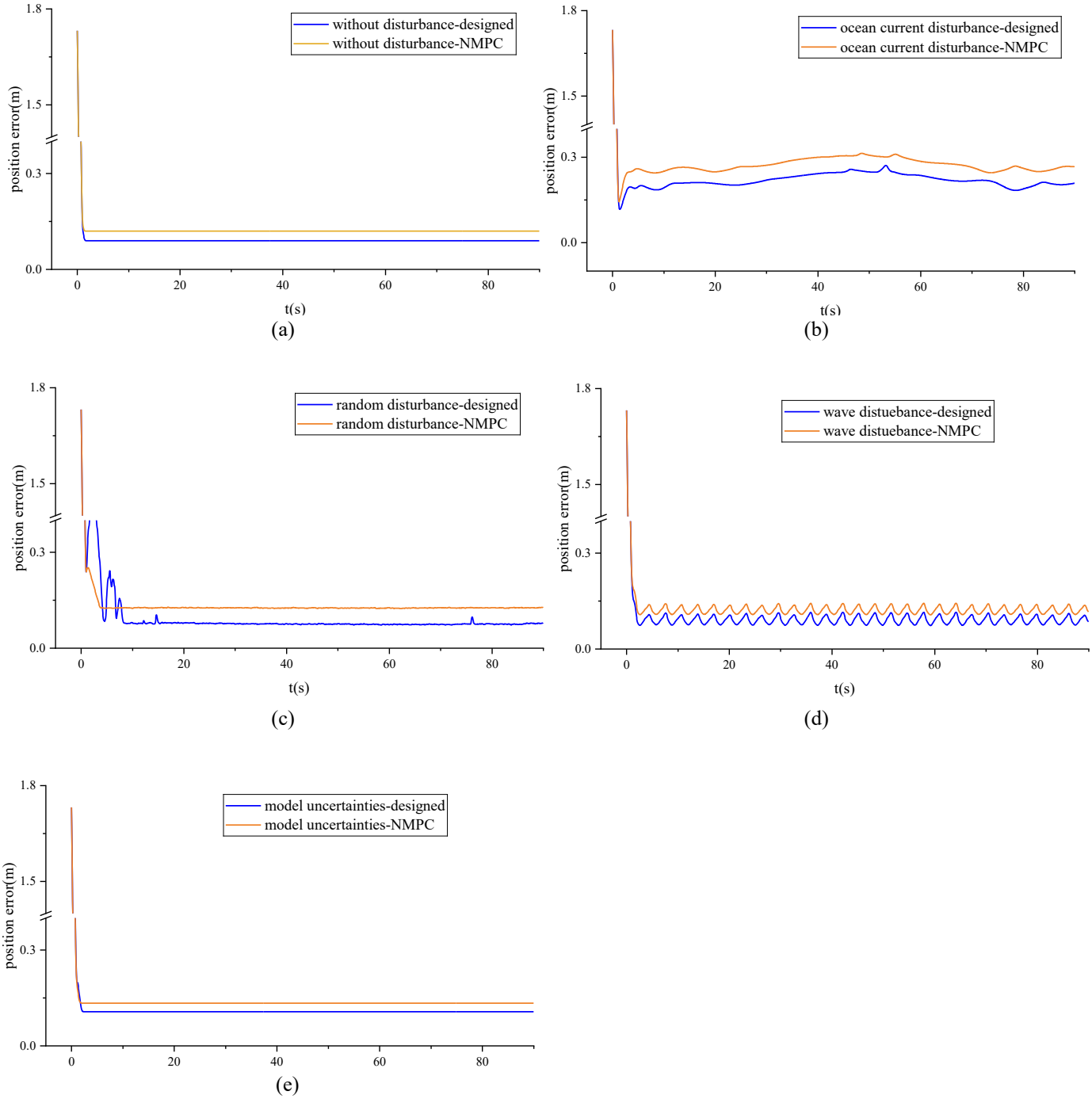

Fig.11 The time history curve of trajectory error value under different disturbances

Fig. 11 displays the time history curve of the helix trajectory error under different disturbances. The tracking error for the newly designed controller is consistently smaller than that of the NMPC controller. Additionally, the trajectory error history is smooth and the overall error remains bounded, demonstrating the effectiveness and stability of the design method. Notably, there is no overshoot in the initial stage.

The tracking error history for the spiral curve does not exhibit periodic changes. This is attributed to the fact that the spiral curve maintains a constant curvature in the $Z_eO_eY_e$ plane and continuously undergoes rotational posture changes. Consequently, the tracking error in this simulation is notably larger compared to the three-dimensional sine curve, which has periodic inflection points only in the Z direction. This distinction is further illustrated in Fig. 12.

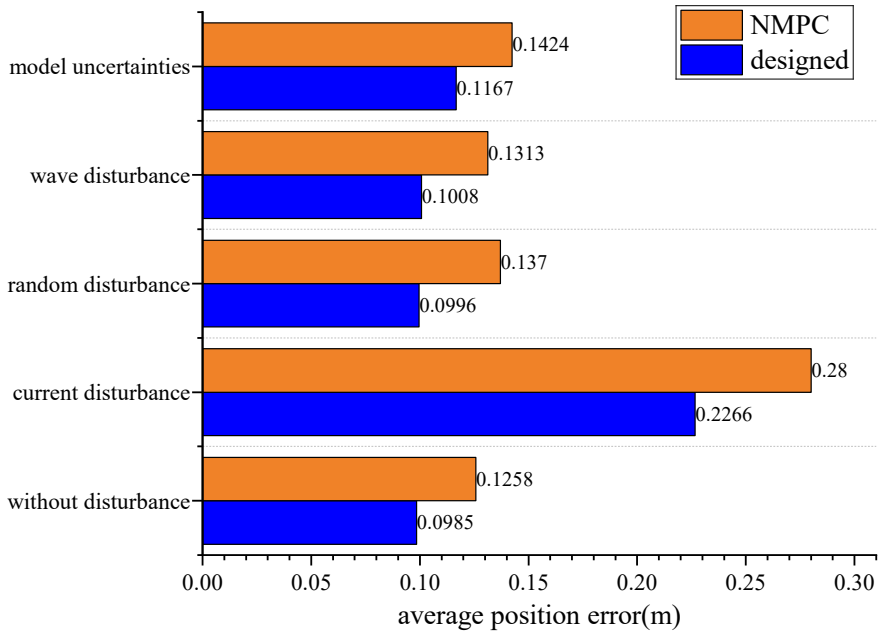

Fig.12 Comparison of tracking error between the designed and the NMPC method

Consistent with previous conclusions, the introduction of disturbances increases the overall position error. However, compared to the sinusoidal trajectory, the position error for the spiral trajectory is significantly greater. As illustrated in Fig. 10(a) the increase in error is attributed to the circular nature of the trajectory curve in the $Y_eO_eZ_e$ plane and the continuous rotational motion of the ROV.

Both controllers are capable of completing the trajectory tracking task even under disturbances. Fig. 12 shows a quantitative comparison and analysis of the average error. The hybrid controller reduces the position error by 19.1%, 27.3%, 23.2%, and 18.0% under these disturbances compared to the baseline controller. In the absence of disturbances, the error is reduced by 23.3%.

Fig. 13 illustrates the variation in output forces and torques across all six degrees of freedom under various operating conditions.

This chapter evaluates the trajectory tracking performance of both controllers by simulating their behavior with two distinct three-dimensional curves across multiple operating scenarios. The comparison between the designed hybrid adaptive controller and the NMPC controller is conducted, with a detailed analysis of their performance characteristics. The results indicate that the hybrid adaptive controller significantly improves trajectory tracking accuracy compared to the NMPC controller.

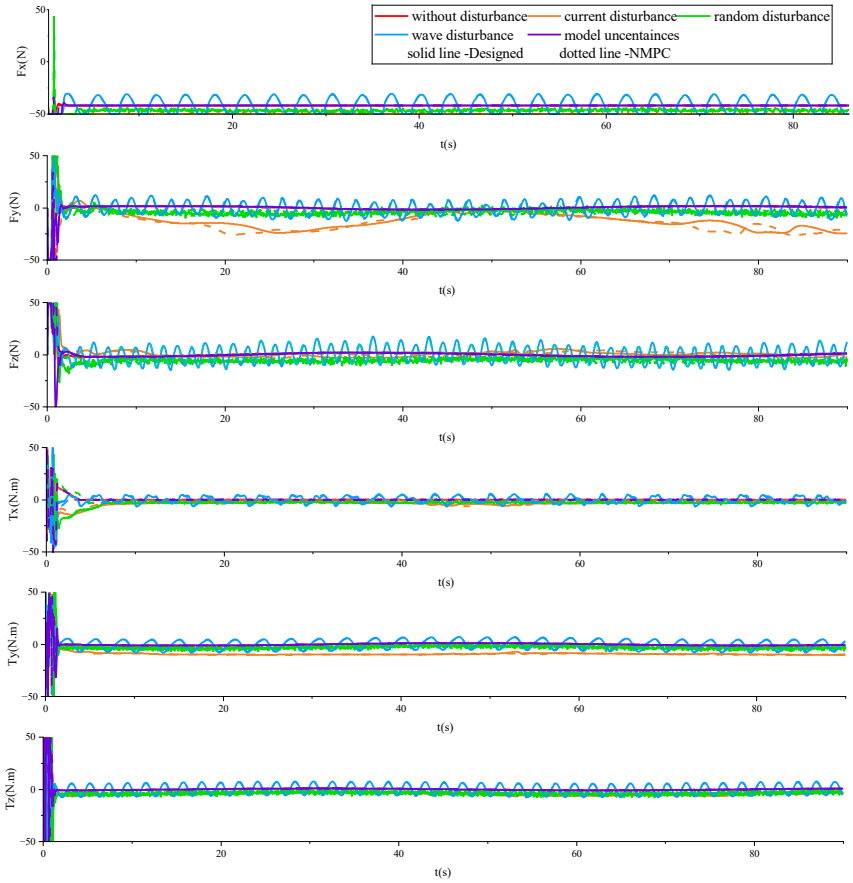

Fig.13 The designed control & NMPC actual output force and torque time history diagram

4. Conclusion

A novel mixed adaptive strategy for three-dimensional trajectory tracking is proposed in this paper. The approach begins with an analysis of the kinematics for a fully-actuated ROV, leading to the development of a 6-DOF nonlinear kinematic and dynamic model. The tracking control problem is then reformulated as an online solvable nonlinear optimization problem using an NMPC controller. The proposed hybrid adaptive controller integrates a new L1 adaptive component with the NMPC method. This combination enhances the disturbance suppression capabilities of the baseline NMPC controller, thereby improving control accuracy. Recognizing the various disturbances that an ROV might encounter in complex marine environments, this study includes simulations for two three-dimensional trajectories under four conditions: random disturbance, ocean current disturbance, wave disturbance, and model uncertainties. The L1 adaptive component, cascaded with the NMPC controller, effectively compensates for tracking disturbances at each sampling interval, enabling the ROV to maintain high performance in the presence of environmental and model parameter errors. Numerical simulations reveal that the position error for the three-dimensional sine curve is reduced by 23.4%, 17.2%, 21.8%, and 22.6% under these four conditions, respectively, compared to the basic NMPC controller. Similarly, for the three-dimensional helix curve, the position error is reduced by 19.1%, 27.3%, 23.2%, and 18.0% under the same disturbances. Notably, the new controller performs even better under model parameter uncertainty compared to the NMPC controller with accurate model parameters. These results validate the effectiveness and robustness of the new hybrid adaptive controller in handling unknown disturbances and model uncertainties.

This paper, based on the foundation of NMPC, introduces an L1 adaptive component to improve control performance, especially in situations with unknown environmental disturbances and model uncertainties. By enhancing NMPC performance, increasing robustness, improving control performance, and introducing

innovative elements in control strategies, this hybrid adaptive control method is not only suitable for ROVs, but also broadly applicable to other autonomous systems operating in complex and uncertain environments.

Acknowledgment

This paper is funded by the National Key Research and Development Program (2022YFC2805200).

REFERENCES

[1] Wang, Z., Wei, Z., Yu, C., Cao, J., Yao, B., Lian, L., 2023. Dynamic modeling and optimal control of a positive buoyancy diving autonomous vehicle. *Brodogradnja*, 74(1), 19-40. https://doi.org/10.21278/brod74102

[2] Yang, L., Xiang, X, Kong, D., Yang, S., 2024. Small Modular AUV Based on 3D Printing Technology: Design, Implementation and Experimental Validation. *Brodogradnja*, 75(1), 75104. https://doi.org/10.21278/brod75104

[3] Yuh, J., 2000. Design and Control of Autonomous Underwater Robots: A Survey. *Autonomous Robots*, 8, 7-24, https://doi.org/10.1023/A:1008984701078

[4] Fossen, T.I., 2002. Marine Control Systems Guidance, Navigation, and Control of Ships, Rigs and Underwater Vehicles. *Springer.*

[5] Ludvigsen, M., Søreide, F., Aasly, K., Ellefmo, S., Zylstra, M., Pardey, M., 2017. ROV based drilling for deep sea mining exploration. *Proceedings of the OCEANS 2017*, 19-22 June, Aberdeen, UK, 1-6. https://doi.org/10.1109/OCEANSE.2017.8084796

[6] Fossen, T.I., 1994. Guidance and control of ocean vehicles. *Wiley*.

[7] Tsukioka, S., Aoki, T., Yamamoto, I., Yoshida, H., Hyakudome, T., Sawa, T., Ishibasi, S., Mizuno, M., Tahara, J., Ishikawa, A., 2005. The PEM fuel cell system for autonomous underwater vehicles. *Marine Technology Society Journal*, 39(3), 56-64. https://doi.org/10.4031/002533205787442558

[8] Kato, N., Short, R., Ukita, M., Senga, H., Yoshie, M., Kobayashi, E., Chiba, H., 2015, Vertical Water Column Survey in the Gulf of Mexico Using Autonomous Underwater Vehicle SOTAB-I. *Marine Technology Society Journal*, 49(3), 88-101. https://doi.org/10.4031/MTSJ.49.3.8

[9] Nian, R., He, B., Yu, J., Bao, Z., Wang, Y., 2013. ROV-based Underwater Vision System for Intelligent Fish Ethology Research. *International Journal of Advanced Robotic Systems,* 10, 326. https://doi.org/10.5772/56800

[10] Liu, J., Wu, S., Yue, X., Yue, Q., 2024. Hydrodynamic shape optimization of an autonomous and remotely-operated vehicle via a multi-surrogate model. *Brodogradnja*, 75(3), 75301. https://doi.org/10.21278/brod75301

[11] Berg, V., 2012. Development and Commissioning of a DP system for ROV SF 30k. *Master thesis*, Norwegian University of Science and Technology.

[12] Soylu, S., Proctor, A.A., Podhorodeski, R.P., Bradley, C., Buckham, B.J., 2016. Precise trajectory control for an inspection class ROV. *Ocean Engineering*, 111, 508-523. https://doi.org/10.1016/j.oceaneng.2015.08.061

[13] Boehm, J., Berkenpas, E., Shepard, C., Paley, D.A., 2021. Tracking Performance of Model-Based Thruster Control of a Remotely Operated Underwater Vehicle. *IEEE Journal of Oceanic Engineering*, 46, 389-401, https://doi.org/10.1109/JOE.2020.2986593

[14] Chu, Z., Zhu, D., Eu Jan, G., 2016. Observer-based adaptive neural network control for a class of remotely operated vehicles. *Ocean Engineering*, 127, 82-89. https://doi.org/10.1016/j.oceaneng.2016.09.038

[15] Caccia, M., Veruggio, G., 2000. Guidance and control of a reconfigurable unmanned underwater vehicle. *Control Engineering Practice*, 8, 21-37. https://doi.org/10.1016/S0967-0661(99)00125-2

[16] Elmokadem, T., Zribi, M., Youcef-Toumi, K., 2017. Terminal sliding mode control for the trajectory tracking of underactuated Autonomous Underwater Vehicles. *Ocean Engineering*, 129, 613-625. https://doi.org/10.1016/j.oceaneng.2016.10.032

[17] Li, M., Yu, C., Zhang, X., Liu, C., Lian, L., 2023. Fuzzy adaptive trajectory tracking control of work-class ROVs considering thruster dynamics. *Ocean Engineering*, 267, 113232. https://doi.org/10.1016/j.oceaneng.2022.113232

[18] Dai, J., Zhao, X., Tan, M., 2002. Fuzzy logic control in autonomous ROV navigation. *Proceedings of the 2002 IEEE Region 10 Conference on Computers, Communications, Control and Power Engineering, TENCOM '02*, 28-31 October, Beijing, China, 1563, 1566-1569. https://doi.org/10.1109/TENCON.2002.1182629

[19] Mon, Y.-J., Lin, C.-M., 2012. Supervisory Recurrent Fuzzy Neural Network Guidance Law Design for Autonomous Underwater Vehicle. *International Journal of Fuzzy Systems*, 14(1), 54-64.

[20] Fossen, T.I., 2011. Motion Control Systems. *Handbook of Marine Craft Hydrodynamics and Motion Control*, 343-415. https://doi.org/10.1002/9781119994138.ch12

[21] Cui, R., Yang, C., Li, Y., Sharma, S., 2017. Adaptive Neural Network Control of AUVs With Control Input Nonlinearities Using Reinforcement Learning. *IEEE Transactions on Systems, Man, and Cybernetics: Systems*, 47, 1019-1029, https://doi.org/10.1109/TSMC.2016.2645699

[22] Cao, Y., Li, B., Li, Q., Stokes, A.A., Ingram, D.M., Kiprakis, A., 2020. A Nonlinear Model Predictive Controller for Remotely Operated Underwater Vehicles With Disturbance Rejection. *IEEE Access*, 8, 158622-158634, https://doi.org/10.1109/ACCESS.2020.3020530

[23] Shen, C., Shi, Y., Buckham, B., 2017. Integrated Path Planning and Tracking Control of an AUV: A Unified Receding Horizon Optimization Approach. *IEEE/ASME Transactions on Mechatronics*, 22, 1163-1173, https://doi.org/10.1109/TMECH.2016.2612689

[24] Gong, P., Yan, Z., Zhang, W., Tang, J., 2021. Lyapunov-based model predictive control trajectory tracking for an autonomous underwater vehicle with external disturbances. *Ocean Engineering*, 232, 109010, https://doi.org/10.1016/j.oceaneng.2021.109010

[25] Bai, G., Meng, Y., Liu, L., Luo, W., Gu, Q., Liu, L., 2019. Review and Comparison of Path Tracking Based on Model Predictive Control. *Electronics*, 8(10), 1077. https://doi.org/10.3390/electronics8101077

[26] Yan, Z., Gong, P., Zhang, W., Wu, W., 2020. Model predictive control of autonomous underwater vehicles for trajectory tracking with external disturbances. *Ocean Engineering*, 217, 107884. https://doi.org/10.1016/j.oceaneng.2020.107884

[27] Zhang, Y., Liu, X., Luo, M., Yang, C. 2019, MPC-based 3-D trajectory tracking for an autonomous underwater vehicle with constraints in complex ocean environments. Ocean Engineering 189, 106309. https://doi.org/10.1016/j.oceaneng.2019.106309

[28] Molero, A., Dunia, R., Cappelletto, J., Fernandez, G., 2011. Model predictive control of remotely operated underwater vehicles. *Proceedings of the 50th IEEE Conference on Decision and Control and European Control Conference*, 12-15 December, Orlando, Florida, USA, 2058-2063. https://doi.org/10.1109/CDC.2011.6161447

[29] Zhu, B., Xia, X., 2016, Adaptive Model Predictive Control for Unconstrained Discrete-Time Linear Systems With Parametric Uncertainties. *IEEE Transactions on Automatic Control*, 61, 3171-3176. https://doi.org/10.1109/TAC.2015.2505783

[30] Gao, J., Liu, C., Proctor, A., 2016. Nonlinear model predictive dynamic positioning control of an underwater vehicle with an onboard USBL system. *Journal of Marine Science and Technology*, 21, 57-69. https://doi.org/10.1007/s00773-015-0332-3

[31] Long, C., Qin, X., Bian, Y., Hu, M., 2021. Trajectory tracking control of ROVs considering external disturbances and measurement noises using ESKF-based MPC. *Ocean Engineering*, 241, 109991, https://doi.org/10.1016/j.oceaneng.2021.109991

[32] Kharisov, E., Hovakimyan, N., Åström, K.J., 2010. Comparison of Several Adaptive Controllers According to Their Robustness Metrics. *AIAA Guidance, Navigation, and Control Conference*, 2-5 August, Toronto, Ontario, Canada. https://doi.org/10.2514/6.2010-8047

[33] Jafari, S., Ioannou, P.A., Rudd, L., 2013. What is L1 Adaptive Control. *AIAA Guidance, Navigation, and Control (GNC) Conference,* 19-22 August, Boston, Massachusetts, USA. https://doi.org/10.2514/6.2013-4513

[34] Gregory, I., Cao, C., Xargay, E., Hovakimyan, N., Zou, X., 2009. L1 adaptive control design for NASA AirSTAR flight test vehicle. *AIAA Guidance, Navigation, and Control Conference*, 10-13 August. Chicago, Illinois, USA. https://doi.org/10.2514/6.2009-5738

[35] Kaminer, I.I., Pascoal, A.M.S., Xargay, E., Hovakimyan, N., Cao, C., Dobrokhodov, V., 2012. Path Following for Unmanned Aerial Vehicles Using L1 Adaptive Augmentation of Commercial Autopilots. *Journal of Guidance, Control, and Dynamics*, 33(2), 550-564. https://doi.org/10.2514/1.42056

[36] Li, Z., Hovakimyan, N., 2012. L1 adaptive controller for MIMO systems with unmatched uncertainties using modified piecewise constant adaptation law. *51st IEEE Conference on Decision and Control, CDC 2012*, 10-13 December, Maui, Hawaii, USA, 7303-7308. https://doi.org/10.1109/CDC.2012.6425935

[37] Pravitra, J., Ackerman, K.A., Cao, C., Hovakimyan, N., Theodorou, E.A., 2020. $\mathscr{L}1$-Adaptive MPPI Architecture for Robust and Agile Control of Multirotors. *IEEE/RSJ International Conference on Intelligent Robots and Systems (IROS)*, 25-29 October, Las Vegas, Nevada, USA 7661-7666. https://doi.org/10.1109/IROS45743.2020.9341154

[38] Xargay, E., Hovakimyan, N., Cao, C., 2010. L1 adaptive controller for multi-input multi-output systems in the presence of nonlinear unmatched uncertainties. *Proceedings of the 2010 American Control Conference*, 30 June-2 July, 874-879. https://doi.org/10.1109/ACC.2010.5530686

[39] Wu, Z., Cheng, S., Ackerman, K.A., Gahlawat, A., Lakshmanan, A., Zhao, P., Hovakimyan, N., 2022. L1Adaptive Augmentation for Geometric Tracking Control of Quadrotors. *Proceedings of the 2022 International Conference on Robotics and Automation (ICRA)*, 23-27 May, 1329-1336. https://doi.org/10.1109/ICRA46639.2022.9811946

[40] Fossen, T.I., 2011. Kinematics. *Handbook of Marine Craft Hydrodynamics and Motion Control*, 15-44. https://doi.org/10.1002/9781119994138.ch2

[41] Fossen, T., Fjellstad, O.E., 1995. Nonlinear Modelling of Marine Vehicles in 6 Degrees of Freedom. *Mathematical Modelling of Systems*, (1)1. https://doi.org/10.1080/13873959508837004

[42] Nguyen, N.T., Prodan, I., Lefèvre, L., 2021. Stability Guarantees for Translational Thrust-Propelled Vehicles Dynamics Through NMPC Designs. *IEEE Transactions on Control Systems Technology*, 29, 207-219, https://doi.org/10.1109/TCST.2020.2974146

[43] Chen, H., AllgöWer, F., 1998. A Quasi-Infinite Horizon Nonlinear Model Predictive Control Scheme with Guaranteed Stability. *Automatica,* 34, 1205-1217, https://doi.org/10.1016/S0005-1098(98)00073-9

[44] Hanover, D., Foehn, P., Sun, S., Kaufmann, E., Scaramuzza, D., 2022. Performance, Precision, and Payloads: Adaptive Nonlinear MPC for Quadrotors. *IEEE Robotics and Automation Letters*, 7, 690-697, https://doi.org/10.1109/LRA.2021.3131690

[45] Lewis, F.L., 2011. L1 Adaptive Control Theory: Guaranteed Robustness with Fast Adaptation. *IEEE Control Systems Magazine*, 31, 112-114, https://doi.org/10.1109/MCS.2011.941837

[46] Wu, C.-J., 2018. 6-DoF Modelling and Control of a Remotely Operated Vehicle. *Master thesis*, College of Science and Engineering, Flinders University.